Available online at www.sciencedirect.com

SCIENCE DIRECT®

Earth and Planetary Science Letters 226 (2004) 17–31

EPSL

www.elsevier.com/locate/epsl

Variations in elastic thickness in the Canadian Shield

Pascal Audet, Jean-Claude Mareschal*

GEOTOP-UQAM-McGILL, Centre de Recherche en Géochimie et Géodynamique, Université du Québec à Montréal, C.P. 8888, succ. "Centre-ville", Montréal, QC, Canada H3C3P8

Received 16 April 2004; received in revised form 15 June 2004; accepted 23 July 2004
Editor: R. van der Hilst

Abstract

We have compared different spectral methods (the standard windowed Fourier transform, the multitaper method (MTM), and the maximum entropy method (MEM)) to determine the coherence between Bouguer gravity and topography and estimate the variations of the effective elastic thickness (T_e) of the lithosphere. These methods differ significantly in spatial resolution (1000 to 2000 km) determined by the width of the windows required to resolve the wavelength of transition from low to high coherence. The tests with synthetic data show that the standard deviation on elastic thickness estimates is high with the three methods but that the mean value obtained by the maximum entropy is close to the input value, while the other methods underestimate the elastic thickness.

In the Canadian Shield, the effective elastic thickness values vary from ≈40 km to >100 km over distances less than the width of the moving window. There is no clear geographical or geological pattern in these variations as high and low elastic thickness values are found near the edge as well as in the center of the continent, and in all provinces regardless of their age. Correlation between T_e and the heat flow field is weak. The values of T_e being much higher beneath Hudson Bay than the Williston Basin are consistent with models of basin evolution and seismic estimates of mantle temperatures.

Keywords: lithosphere; elastic thickness; gravity; isostasy

1. Introduction

The level of isostatic compensation of the continental lithosphere depends on its composition and thermal regime that affect its long-term mechanical properties. Flexural isostasy assumes that the response of the lithosphere to loading can be modeled as that of a thin elastic plate with known mechanical properties overlying an inviscid fluid [1]. This approach supposes that gravitational equilibrium of the lithosphere can be maintained over geological time and space scales. Compensation is achieved by the deflection of the plate in response to surface and internal loads. For

* Corresponding author. Tel.: +514 987 3000x6864; fax: +514 987 3635.
E-mail address: jcm@olympus.geotop.uqam.ca (J.-C. Mareschal).

0012-821X/$ - see front matter © 2004 Elsevier B.V. All rights reserved.
doi:10.1016/j.epsl.2004.07.035

a thin elastic plate of given thickness and elastic properties, the response to loading is characterized by a single parameter, the flexural rigidity, D,

$$D = \frac{ET_e^3}{12(1-\nu^2)}, \quad (1)$$

where E is Young's modulus, T_e is the plate thickness and ν is Poisson's ratio. The effective elastic thickness of the lithosphere is defined as the thickness of an equivalent elastic plate which would produce the same deflection under the known tectonic loading structure. This parameter depends on a large number of geophysical properties such as the stresses acting on the plate, its thermal state, composition and geometry [2].

In the oceans, where the composition and thermal evolution of the lithosphere are relatively simple, T_e is given approximately by the depth to the 450–600 °C oceanic isotherm based on the cooling plate model [3]. The composition and thermal regime of continental lithosphere are more complicated than for the oceans and there has been much debate on the meaning of T_e for the continents. In general, T_e is low in young and tectonically active regions [4] and is expected to be high in cratons where high values are usually found [5], but low values have also been reported [6].

Flexural rigidity of lithosphere can be estimated by direct modelling of the plate response to loading when the load is well known. This is the situation for seamounts [3], sedimentary basins [7], or some mountain belts [8]. Analysis of the correlation between the topography and the gravity data, either free air or Bouguer anomaly, with spectral methods provides an alternative to direct modeling. The free air anomaly is a signal corrected for gravity effects caused by the elevation difference between the stations where measurements are taken and sea level. The Bouguer anomaly is further corrected for topographic effects. The first attempt to study the isostatic compensation mechanism from the spectral properties of both the gravity field and topography was made by Lewis and Dorman [9]. In their study, they assumed that a linear transfer function between topography and Bouguer gravity, the admittance, can be used to describe the mechanism of isostatic compensation. They calculated the admittance in the wavenumber domain for the continental US and inverted this admittance to infer the depth of the compensating density interface. Their results suggested that compensation occurs at a depth of ≈ 200 km. Banks et al. [10] showed that the assumption of local compensation (i.e. no flexural rigidity) had affected these results and that, with a model of regional compensation (i.e. loads are compensated by the flexure of an elastic plate), most of the compensation takes place at Moho depth. They inverted the admittance to estimate the flexural rigidity of the lithosphere. Some estimates of the elastic thickness of the continental lithosphere based on the admittance were surprisingly low, suggesting that even cratons have no mechanical strength [6]. These results were later questioned by Forsyth [11] who showed that the elastic thickness estimated by the admittance method yields too low T_e values if internal loads are not taken into account. He suggested that the coherence between Bouguer gravity and topography yields better estimates of T_e than the admittance, because it allows to distinguish between internal and external loads and it is more sensitive to the elastic thickness than to the loading structure. Following this work of Forsyth [11], the coherence method has been preferred and routinely used by the majority of researchers, with the notable exception of McKenzie and Fairhead [12] who claim that elastic thickness is better estimated from the admittance between topography and free air gravity, especially in the case where erosion has obliterated surface loads without subsequent reequilibration. Recently, Perez-Gussinye et al. [13] reformulated the free-air admittance method and obtained results similar to those obtained with the Bouguer coherence, although its performance is judged to be poor. One of the problems with the free-air admittance relates to its higher sensitivity to short-wavelength noise and to unaccounted near-surface density variations. Bouguer-based methods are less sensitive to data resolution, and thus, we prefer the coherence method using Bouguer gravity to compute T_e.

The main objective of this paper is to analyze the variations of the effective elastic thickness in the Canadian Shield. Previous studies aimed at computing the elastic thickness in parts of Canada showed that the effective elastic thickness is large over most of the Shield [5,14–16]. The suggestion that there is

a systematic increase in elastic thickness from the Atlantic and Labrador Sea toward the Central part of the Shield [5] has not been confirmed by more detailed studies using different spectral methods [15]. These studies show that elastic thickness varies on a scale of 1000 km without any relationship to surface geology or geography. The elastic thickness is much lower in the active western Canadian Cordillera where heat flow and lithospheric temperatures are higher than in the Shield [16]. Other studies, e.g. of the Australian lithosphere [17], show a first-order correlation of elastic thickness with crustal age on length scales larger than 1000 km, with significant deviations from this trend on smaller length scales.

In cratonic areas, where the effective elastic thickness has been reported to exceed 100 km, e.g. in Western Canada [16] or in Australia [18], the transition from un-compensated to compensated loads occurs at very long wavelengths (several hundred kilometers, depending on the ratio of surface to subsurface loading, see Eqs. (4–6) in Simons and van der Hilst [19]). The selection of a spectral estimator is critical because very wide windows are required to resolve these wavelengths. We have tested different spectral estimators (standard periodogram, multitaper [20], and the maximum entropy method [4]) with synthetic data to determine which method suits best our purpose and provides the highest resolution. These tests show that the maximum entropy method has a better spatial resolution than the other methods which require wide windows in order to estimate the spectra when T_e is large. We have thus retained the maximum entropy method to map the variations of the elastic thickness in the Canadian Shield that can be compared with relevant geological and geophysical data.

2. Tectonic setting

The present architecture of the Canadian Shield is the result of the early Proterozoic (1.8 Ga) welding of several Archean cratons [21]. The last major tectonic event in the Canadian Shield was the Grenville orogeny which culminated at 1.1 Ga. The main tectonic boundaries of the Canadian Shield can be identified on the gravity map (Fig. 1). The central part of the Canadian Shield, and the largest of the Archean blocks, is the Superior craton that stabilized before 2.5 Ga. The Superior Province (SUP) is exposed in northern Ontario and Manitoba to the west and in the northern part of Québec.

West and north of the Superior Province, two Archean blocks (the Hearne and the Rae provinces) are separated from the Superior by the Early Proterozoic Trans-Hudson orogen (THO). The THO is exposed only in northern Manitoba and Saskatchewan, but it can be traced under the sedimentary cover of the Williston and Hudson Bay Basins from the Dakotas to the Cape Smith Belt at the northern tip of Québec. The different Belts of the THO include mostly juvenile rocks (derived from the mantle) of oceanic affinity, but in the southern part of the THO, these juvenile rocks were transported over a small Archean block, the Sask craton [22]. West of the exposed part of the Shield, the Hearne and Rae Provinces extend beneath the western Canada sedimentary basin.

To the east, the Superior is separated from the Archean Nain Province, by the southeastern Churchill Province which consists of a core zone of reworked Archean rocks sandwiched between the New Quebec and the Torngat orogens [23]. The Nain Province is a part of the North Atlantic craton from which it was separated by the opening of the Labrador Sea at 100 Ma.

South of the Superior Province, the Grenville Province is a major Mid Proterozoic zone of collision extending from northern Mexico to Labrador. It is separated by the Atlantic ocean from its European counterpart in Scandinavia. The Grenville Front, separating the Grenville Province from the older structural provinces to the northwest, is a sharp northeast trending tectonic break that is well defined on the regional gravity and magnetic maps. The Grenville Province in Canada consists of an autochtonous, and of several allochthonous belts that were emplaced during a series of tectonic events culminating at 1.1 Ga. On the seismic reflection profiles conducted by LITHOPROBE, reflectors that can be identified as the Archean basement extend far south into the Grenville Province. The Canadian Shield disappears beneath

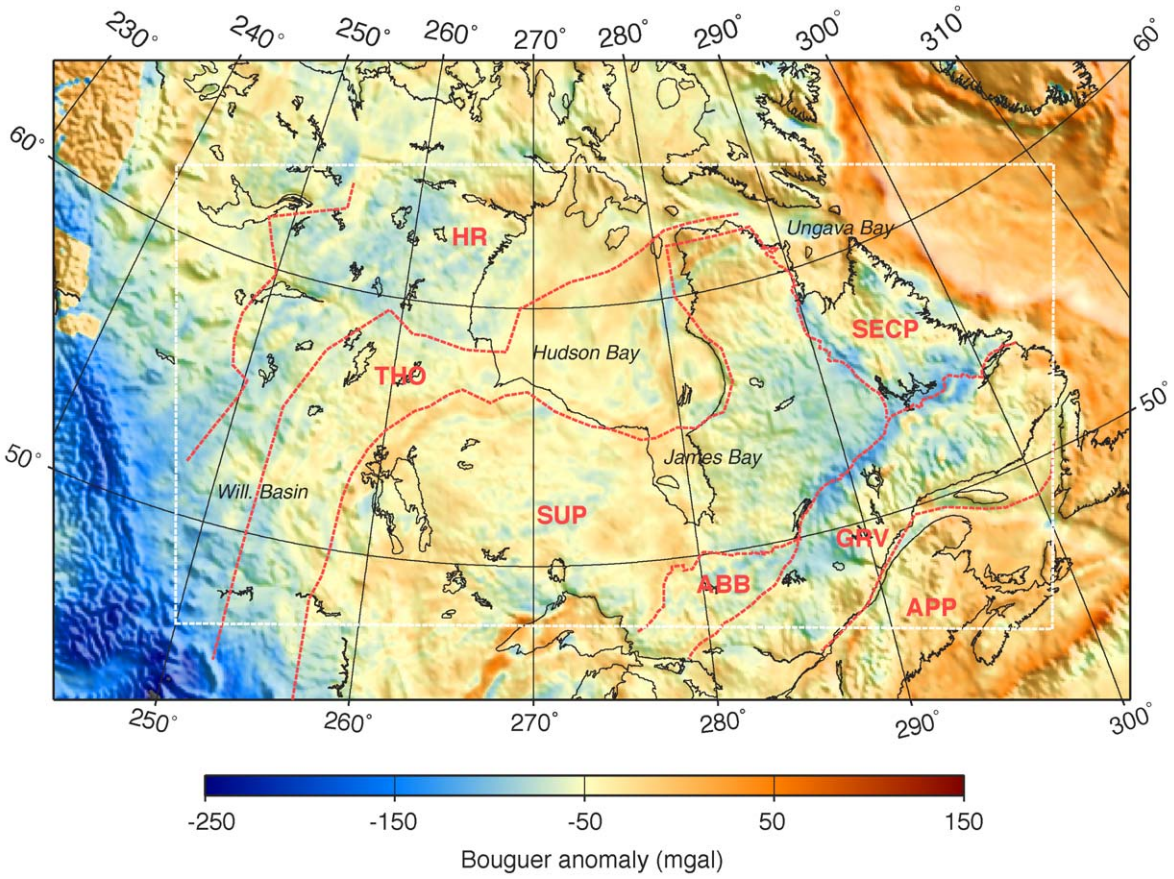

Fig. 1. Gravity map of the Canadian Shield with topography superposed as shaded relief. The main geological provinces are also shown. Archean Provinces (>2.5 Ga): SUP: Superior Province, H–R: Hearne–Rae, ABB: Abitibi greenstone belt; Early Proterozoic Provinces (ca. 1.8 Ga): THO: Trans-Hudson Orogen, SECP: Southeastern Churchill Province; Mid Proterozoic (ca. 1.1 Ga): GRV: Grenville Province. Paleozoic Appalachians (APP) are also shown.

the Paleozoic Appalachians which were thrust over the Grenville basement.

3. Estimating elastic thickness

3.1. Coherence

The coherence method for estimating T_e is based on the assumption that there is no correlation between surface and internal loads, and that such internal loads must be both present and topographically expressed. Short-wavelength loads, due to topography or internal density contrasts, are supported by the strength of the plate and the topography is thus incoherent with the Bouguer gravity anomalies, which reflect a combination of the undulations of the compensating interface as well as the internal loads, from which they are assumed to be independent. For long wavelengths, the deflection of the plate will produce compensation, and the gravity anomaly produced by this flexure will be coherent with the topography. The transition wavelength from low to high coherence depends on the rigidity of the plate as well as on the ratio of bottom-to-top loading f, and is used to determine the elastic thickness of the lithosphere. The fundamental uncertainty is due to the fact that, although f can be estimated from the data, it is most often wavelength-dependent, leading to a non-unique problem.

Although the coherence method has been widely used, the choice of a method for estimating the elastic thickness in continental areas is still debated. For example, McKenzie and Fairhead [12] have argued that the use of the coherence between the Bouguer anomaly and topography yields only upper bounds on T_e when erosion has reduced the topography at intermediate wavelengths, and therefore, the transition from low to high coherence is shifted toward the long wavelengths. Swain and Kirby [24] addressed this problem by simulating the effect of erosion as a decrease in the Bouguer gravity spectrum compared to the free-air gravity spectrum at intermediate wavelengths, but concluded that the effect on T_e estimates obtained with the coherence method is relatively minor. McKenzie [25] further investigated the effects of the presence of internal loads without topographic expression, as a result of erosion or sedimentation. In this case, the basic assumption of the coherence method of Forsyth [11] is violated. Such a situation is likely to occur in the Canadian Shield where there is little topography. However, there is some topography in the Shield and several old tectonic features (Torngat orogen, Grenville Front) have gravity and topographic expressions. Long wavelength gravity anomalies without topography must be supported by the plate rigidity and are consistent with a strong lithosphere.

The observed coherence γ_0 is calculated in the wavenumber domain as

$$\gamma_0^2(k) = \frac{\langle BH^* \rangle^2}{\langle HH^* \rangle \langle BB^* \rangle}, \tag{2}$$

where k is the length of the two-dimensional wavevector, B and H are the spectral representations (Fourier transforms) of the Bouguer gravity and topography fields, the asterisk denotes the complex conjugate and the brackets indicate an averaging procedure. As Simons et al. [20] have shown, this averaging is essential, but it can take many forms. Neglecting a possible anisotropy of the plate strength, most often the averaging is performed by binning the cross-spectral estimate into discrete wavenumber bands.

If the Bouguer gravity anomaly is due to the undulations of the Moho, the topography of the Moho $W(\vec{k})$ can be calculated in wavenumber domain by downward continuation of the Bouguer anomaly $B(\vec{k})$:

$$W(\vec{k}) = \frac{B(\vec{k})}{2\pi G \Delta\rho} \exp(|k| z_m), \tag{3}$$

where G is the gravitational constant, z_m is the estimated mean Moho depth and $\Delta\rho$ is the density jump across the Moho. Both surface and Moho topography can then be decomposed into their components due to surface and sub-surface loading.

For a surface load $H_T - W_T$, the topography of the Moho (due to flexure) W_T is obtained in wavenumber domain as:

$$W_T = \left(\frac{-\rho_c}{\rho_m - \rho_c} \right) \left(\frac{Dk^4}{g(\rho_m - \rho_c)} + 1 \right)^{-1} H_T, \tag{4}$$

and the surface topography H_B caused by flexure due to an internal load $W_B - H_B$ is given by:

$$W_B = \left(\frac{-\rho_c}{\rho_m - \rho_c} \right) \left(\frac{Dk^4}{g\rho_c} + 1 \right) H_B, \tag{5}$$

where D is the flexural parameter, ρ_c and ρ_m are the crustal and mantle density. Eq. (4) and (5) are only valid for constant D.

If the flexural parameter D were known, it would be possible to use the flexural response functions and decompose the topography of the surface $H = H_B + H_T$ and of the Moho $W = W_B + W_T$, into their external (H_T, W_T) and internal components (H_B, W_B) [11]. For a given value of the elastic thickness, we can thus calculate the predicted coherence γ_p if the internal and surface loads are uncorrelated:

$$\gamma_p^2(k) = \frac{\langle H_T W_T + H_B W_B \rangle^2}{\langle H_T^2 + H_B^2 \rangle \langle W_T^2 + W_B^2 \rangle}. \tag{6}$$

For a given value of T_e, the predicted coherence is calculated for each wavenumber band and the misfit is calculated in the L_2 norm:

$$\sum_{i=1}^{N} \left| \left(\gamma_o^2 - \gamma_p^2 \right) \right|^2, \tag{7}$$

where N is the number of wavenumbers analyzed. The T_e value retained is the one that minimizes the misfit. Because the variance of the short-wavelength coherence is small, we chose a non-weighted

criterion for the L_2 norm in order to not down-weight the effect of features near the transition wavelength, which is the portion of the curve most sensitive to T_e.

3.2. Spectral methods

One of the main difficulties in estimating the elastic thickness with the coherence method is that high values of T_e require a very wide window in order to correctly resolve the large transition wavelength in the spectrum. Since it is likely that the plate's elastic behavior may vary on distances shorter than the width of the window, using wide windows may result in averaging out the elastic properties of smaller sub-regions. The choice of the spectral estimator becomes very critical if one wants to map the spatial variations in the elastic properties of the continental lithosphere, where T_e can reach values as high as a hundred kilometers [26]. We have thus first compared the results obtained using three different spectral estimators (the standard periodogram, the multitaper, and the maximum entropy) with synthetic data.

The standard periodogram (SPM) is obtained from the digital Fourier transform of the data. The standard technique to reduce leakage is to apply a suitable taper to the data which forces them to tend to zero at the sides of the window. We have estimated the spectrum from the standard Fourier transform method with a Hanning window.

The SPM possesses the disadvantage of discarding valuable information located at the extremities of the taper. The Welch method bypasses this problem by stacking estimates from overlapping windows applied to the data, but it requires the data set to be much wider than the window. As an alternative to the Welch method, the multitaper method (MTM) applies different tapers to the same data set. These tapers, known as Discrete Prolate Spheroidal Sequences (DPSS), form a set of eigenfunctions, solutions of the variational problem of leakage minimization. Because they are orthogonal, they provide approximately uncorrelated estimates of the spectrum [27] which is calculated by averaging these estimates. The MTM has been in favor for many geophysical applications and used in several recent studies of T_e [12,13,20,24].

Using many tapers on a data set can have undesirable effects while computing the coherence between two fields because the spectral resolution degrades and the leakage increases with the number of tapers used [13]. The coherence is more sensitive to these effects for low wavenumbers because the fixed width of the resolution kernel and the leakage introduced when computing the wavenumber domain convolution between the true power spectrum and the power spectral density of the tapering windows smear out the long wavelength information. These effects increase the coherence for wavelengths near the roll-over, and the transition appears at shorter wavelength than it would, resulting in the rigidity being underestimated. In order to reduce this effect, one can use a set of fewer tapers (which leads to a narrower spectral resolution peak at the low wavenumbers) or use a wider window (which has the same effect). However, since the estimate is a weighted average over the individually tapered estimates, reducing the number of tapers gives a greater variance of the estimate, while increasing the size of the window lowers the spatial resolution. There is a compromise between the window size and the number of tapers used for each region under study. In our tests, we used three tapers in each direction and averaged the 9 two-dimensional spectra only.

The MTM is a non-parametric method. Parametric methods, on the other hand, are based on the assumption that the process that has produced the data is known, usually taken to be an auto-regressive process. If that critical assumption is verified, the width of the data window does not limit the wavelength that can be resolved and a continuous spectrum can be derived from the parameters defining the process. The Burg algorithm [28] to determine the parameters of the auto-regressive process and the spectrum is often referred to as the maximum entropy method (MEM), because the auto-correlation function is minimized outside the region where it can be directly calculated from the data. It is thus possible to obtain information at longer wavelengths than the maximum imposed by the width of the data, potentially resulting in improved spatial resolution because it can use relatively small windows. Following Lowry and Smith [4], several authors [15,16,33] have applied the MEM to estimating the T_e.

The cross and spectra obtained by these three methods can be directly imported into the coherence function and inverted to estimate T_e.

3.3. Tests with synthetic data

Synthetic data were generated from two non-correlated fractal distributions with a spectral slope $\beta=-3$. These two distributions are used as the initial surface and internal loads, which are applied to a plate with variable thickness and fixed elastic properties ($E=1\times10^{11}$ Pa, $\nu=0.25$) [29]. The sub-surface loading is treated as relief on a plane corresponding to the mean Moho depth and the density jump is taken to 500 kg m^{-3}. We can then calculate the resulting topography and Bouguer anomaly at equilibrium by selecting the ratio f of internal to surface loading. We take a constant value of $f=1$ for the generation of our synthetic data sets.

Synthetic data were calculated on 256×256 grids with a sampling interval of 8 km (2048×2048 km^2). The spectra were calculated on a smaller sub-grid (1024×1024 km^2) to avoid the intrinsic periodicity at the edges of the grids and to produce a more realistic set of data. Using this procedure, 50 gravity and topography data sets were generated for each elastic plate thickness of 10, 20, 40, 60, 80, 100 and 120 km. These data sets were then used to determine T_e with the coherence method using three different spectral estimates. In Figs. 2–4, we compare results obtained on synthetic data

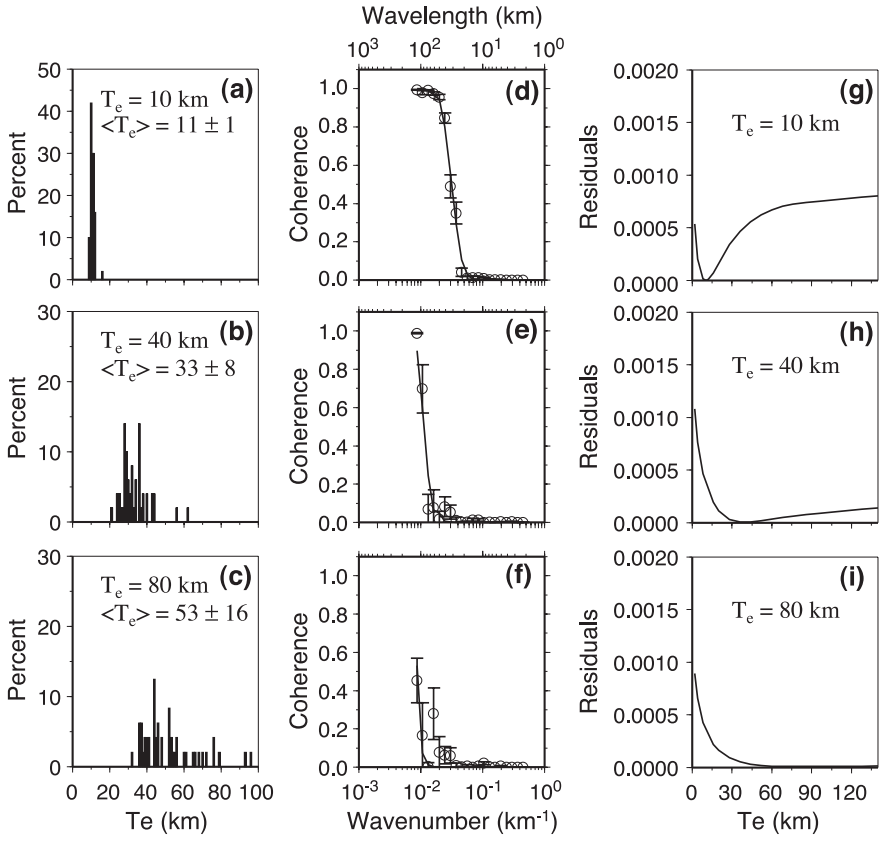

Fig. 2. Results from synthetic data. (a–c) Distributions of estimated T_e for SPM along with examples of observed and predicted coherence curves (d–f) and L_2 norm misfit (g–i) for three different values of T_e (10, 40 and 80 km) using a constant load ratio of $f=1$. The dimension of the square windows is 1024×1024 km^2. The observed coherence is shown as open circles and error bars are one standard deviation. The best fitting predicted coherences, given by the minimum value of the misfit, are shown as solid lines.

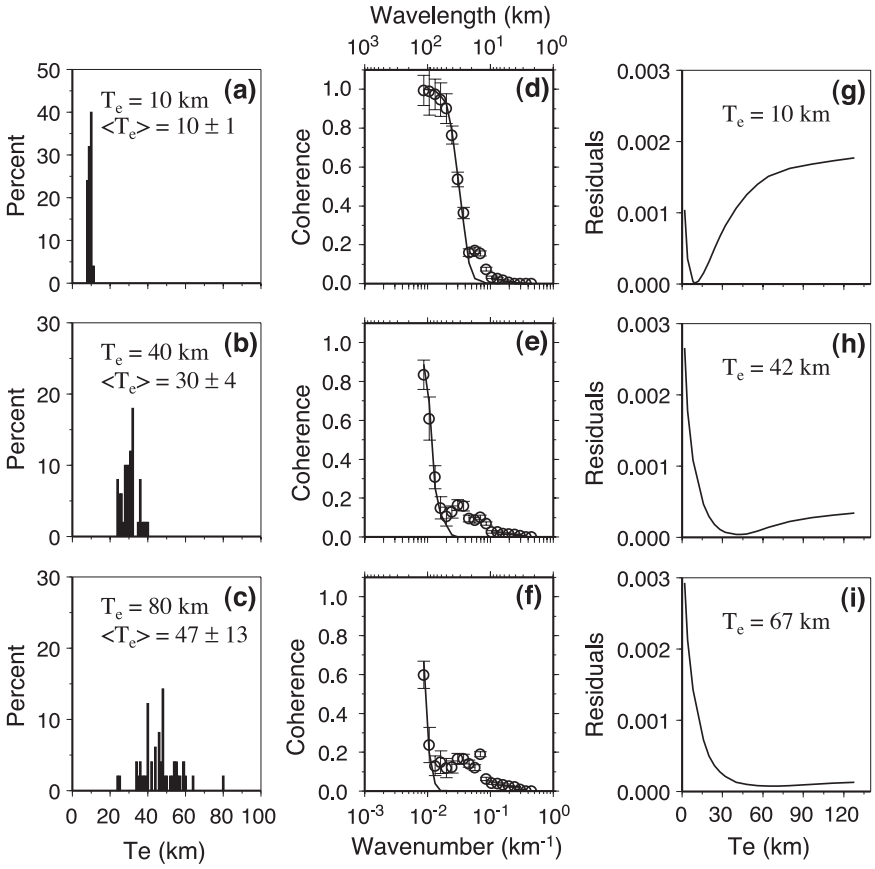

Fig. 3. Same as Fig. 2 with MTM.

with the periodogram, the multitaper, and the maximum entropy methods respectively. For each method, we show results for T_e=10, 40, and 80 km. We show the distributions of T_e estimates for all 50 synthetic data sets, the observed coherence with their mean and standard deviations at each wavenumber and the best fitting predicted coherence, and the L_2 norm misfit. For T_e=10 km, the misfit curve has a well-marked minimum and there is very little scatter on the estimates. With increasing elastic thickness, the minimum is less pronounced and the standard deviation on T_e estimates increases for all three methods. For the SPM and the MTM, the mean of all the estimates is less than the value of T_e used to generate the data. For the MEM, the standard deviation of all the estimates is as large as with the other methods but the mean is close to the value used to generate the synthetic data. This is because both the multitaper and the standard windowed Fourier transform methods poorly resolve long wavelengths (relative to the window width).

In Figs. 2–4d–f, we compare the observed and predicted coherence as a function of wavelength. The circles represent the calculated coherence averaged over wavenumber bins with the associated standard deviation, and the solid line is the best-fitting predicted coherence. The SPM and MTM cannot determine the coherence function at the long wavelengths where it should increase. This is not the case with the MEM. The MEM has this "improved" resolving power because of an assumption on the data set. It is not surprising that this assumption of minimum long range auto-correlation is valid for the synthetic data that were generated as a fractal surface. Whether these conditions remain

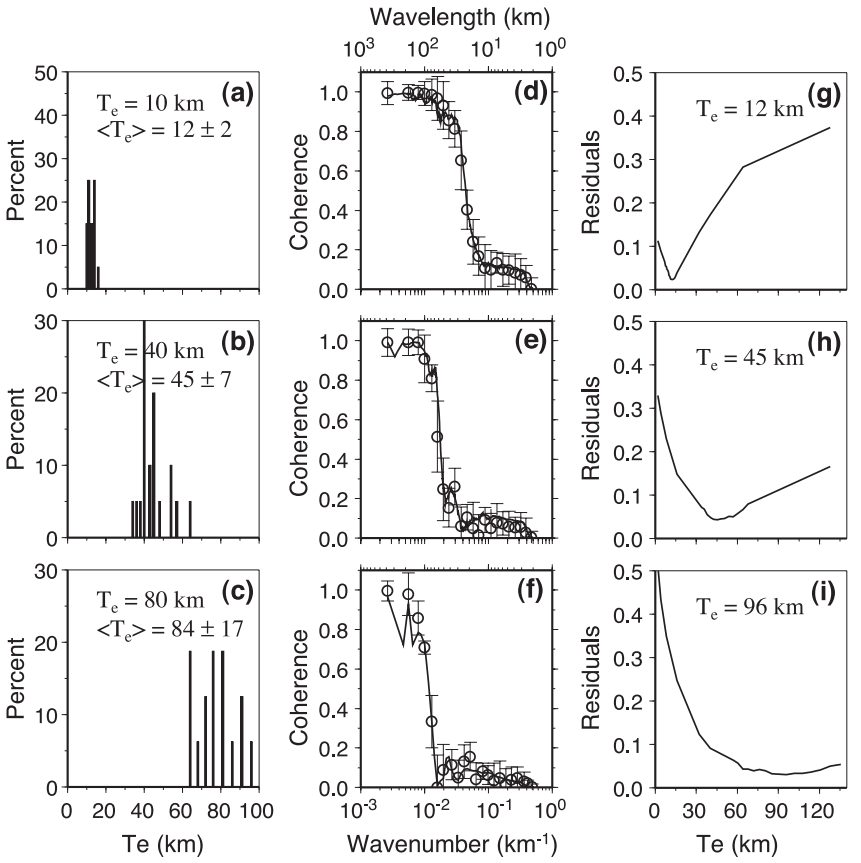

Fig. 4. Same as Fig. 2 with MEM.

valid with real geophysical data remains an open question.

The misfits (Figs. 2–4g–i) illustrate the difficulty in estimating the value of T_e when it is large. For T_e>40 km, the misfit is not very sensitive to the estimated T_e value. All estimates larger than some threshold give the same value for the misfit.

Fig. 5 shows the differences between the value T_e estimated and that used to generate the synthetic data for all three methods. The observed (or apparent) T_e is plotted against the true T_e to show the spatial resolution of each method with increasing values of T_e. The error bars are the standard deviations and the solid curves are second degree polynomials. Clearly, the best approximation is obtained with the MEM because it allows the extrapolation of information for wavelengths greater than the window size. For T_e>40 km, the MTM and SPM underestimate the elastic thickness because the transition wavelength approaches the window size. The relative difference between estimated and true value of T_e increases with T_e. The MTM under-estimates the value of T_e more than the SPM because the large number of tapers smears out the long wavelength information and increases the coherence at these wavelengths, leading to an underestimation of the elastic thickness [13,24].

All the synthetic data sets were generated with a loading ratio f=1 at all wavelengths. When determining the best fit with the MEM method, we found that the loading ratio was always overestimated: for wavelengths <500 km, the mean value of f is ≈1.5, and it increases between 500 and 1500 km to reach ≈3. This error on the loading ratio had very little effect on the estimated T_e.

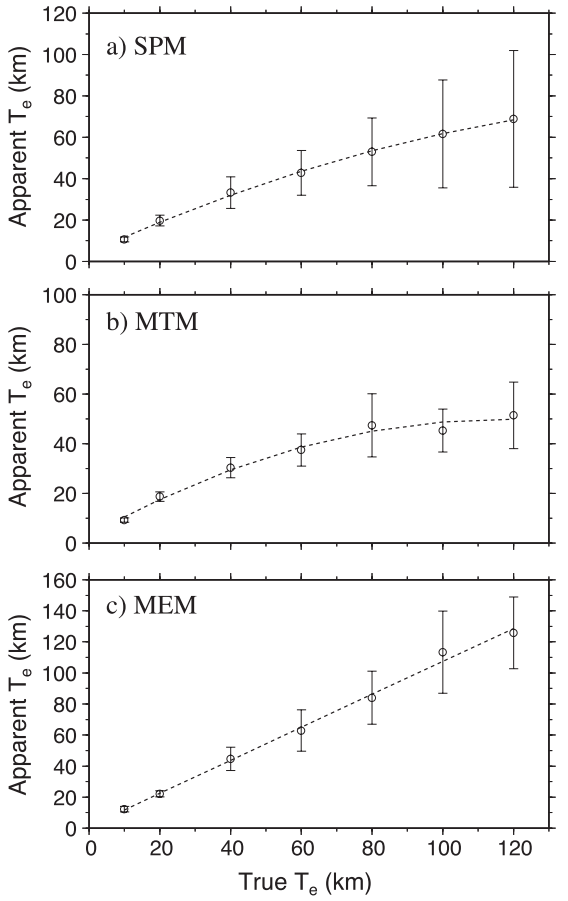

Fig. 5. Calculated misfit for T_e estimations with the three spectral estimators (a—SPM, b—MTM, c—MEM). Each estimate represents an average over 50 runs on synthetic gravity and topography grids of dimensions 1024×1024 km^2, along with the corresponding standard deviation. The dotted lines are second degree polynomials. The best agreement is found with the MEM because it allows the extrapolation of information for wavelengths longer than the window size. The loss of resolution shown with SPM and MTM is due to the width of the window. When the plate has a strong rigidity, these methods are unable to fully resolve the transition wavelength from low to high coherence.

The comparison between the different spectral methods suggests that the maximum entropy method is the only one that can determine values of T_e up to 100 km with a 1024×1024 km^2 grid. Other methods require wider grids and result in less spatial resolution than the MEM. For this reason, we have selected the MEM to determine the variations in T_e in the Canadian Shield.

4. Effective elastic thickness in the Canadian Shield

4.1. Canadian Shield data

The Bouguer gravity data were obtained from the Geological Survey of Canada and from the compilation of the Decade of North American Geology. We have used the free-air gravity data derived from satellite altimetry of Smith and Sandwell [30] to complete the grids over the Ungava Bay region where no standard gravity measurements were made. The free-air gravity data were converted into Bouguer data using the bathymetry and a constant rock density (2640 kg m^{-3}). The topography-bathymetry data come from the 2′ grid digital elevation model of Smith and Sandwell [31].

Our data cover most of the Canadian Shield, part of the western interior platform (Williston and Alberta basins) and a small part of the Appalachians in Canada. The data set was placed on a grid with 8-km sampling distance over an area of 4658×2765 km^2 (Fig. 1). We extracted sub-grids of 128×128 (1024×1024 km^2) to determine the flexural parameter D. In order to calculate T_e from the flexural parameter, we assumed that Poisson's ratio ν=0.25 and that Young modulus E=1×10^{11} Pa. The density increases from 2670 kg m^{-3} at the surface to 3100 kg m^{-3} at the Moho. We used the depth to the Moho from the LITH5.0 crustal density model of Perry et al. [32]. We have calculated T_e for a regular grid with a 256-km distance between nodes. Because the tests with synthetic data have shown that there is large standard deviation on individual elastic thickness estimates, we have tried to reduce the variance by averaging 9 partly overlapping estimates at each node. These estimates are obtained by translating the window 128 km in each direction from the central node. By employing this procedure, we assume implicitly that re-measuring the data on overlapping segments amounts to picking other samples from the same underlying process which have the same standard deviation, hence, we can divide the variance by the number of entries. The standard deviation σ of all estimates for each node is comparable to that obtained in the tests with synthetic data, with σ on the order of 25 km for T_e>80 km, and σ<10 km when T_e<40 km.

4.2. Major trends in T_e

Fig. 6 shows typical examples of the determination of T_e in different parts of the Shield. The misfit curve from the eastern Shield (Fig. 6d) illustrates the difficulty in determining a reliable T_e value when the plate is strong. Because of this large uncertainty, we prefer to discuss the relative variations in T_e rather than their local absolute values.

The map of effective elastic thickness is shown in Fig. 7. The map covers a wider region than that in the study by Wang and Mareschal [15]. The trends are consistent in the regions where the two studies overlap. However, because we have reduced the variance in the present study by averaging independent estimates of T_e at each node, local values may be different between the two maps. The elastic thickness is very variable (<40 to >120 km), but it remains large >40 km throughout the Shield and in the Canadian Appalachians. Values <40 km are found in the western interior platform and the Alberta basin.

In the Shield, the highest values for T_e are found beneath Hudson Bay and the Hearne and Rae cratons, west of Hudson Bay. Values >100 km are also found in the southeastern Superior and eastern Grenville Province as well as west of Lake Superior, in the western part of the Superior Province. In the eastern part of the Shield, T_e values remain large (50 km<T_e<80 km) but are in general lower than in the northwestern Shield and Hudson Bay. In the Superior Province, the lowest values ($\approx$50 km) are found south of James Bay, over most of the Abitibi subprovince. For the Appalachians, T_e is poorly estimated, either because the flexural wavelength is not fully resolved or because we could not obtain a reliable minimum for the L_2 norm misfit. This suggests that T_e is large for the Appalachians. This would be consistent with the analysis by Armstrong and Watts [33] who showed high values for T_e toward the northern part of the Appalachians.

We also calculated the ratio $f(k)$ of the amplitude of sub-surface to surface loading in the Superior Prov-

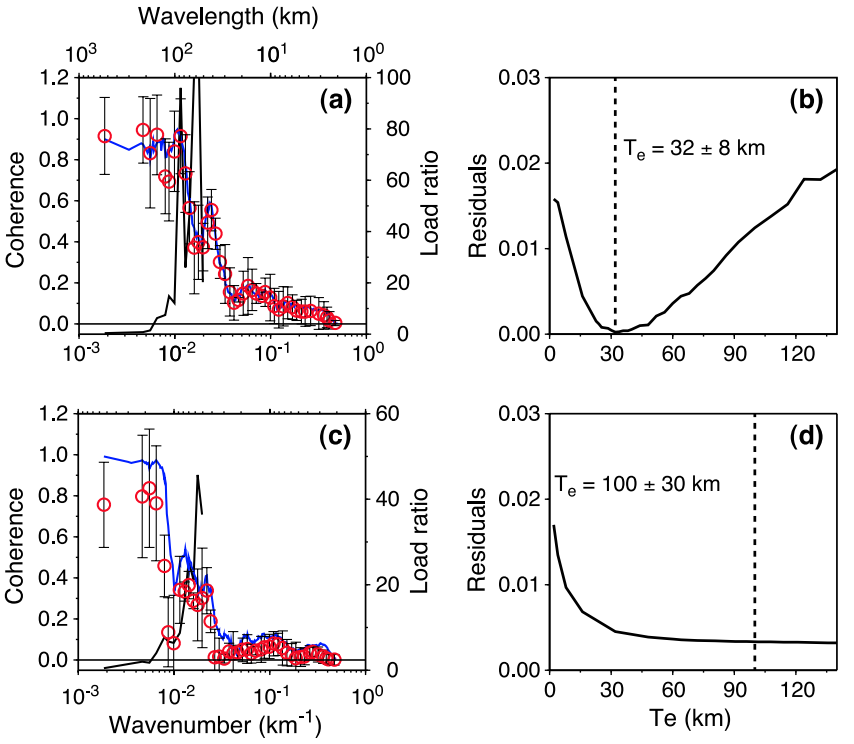

Fig. 6. Examples of observed (red circles) and predicted (blue line) coherence curves along with L_2 norm misfit curves used to estimate T_e. The black curves show the variations with wavelength of the load ratio f (scale on the right). Error bars are one standard deviation. (a–b) western Shield, and (c–d) eastern Shield.

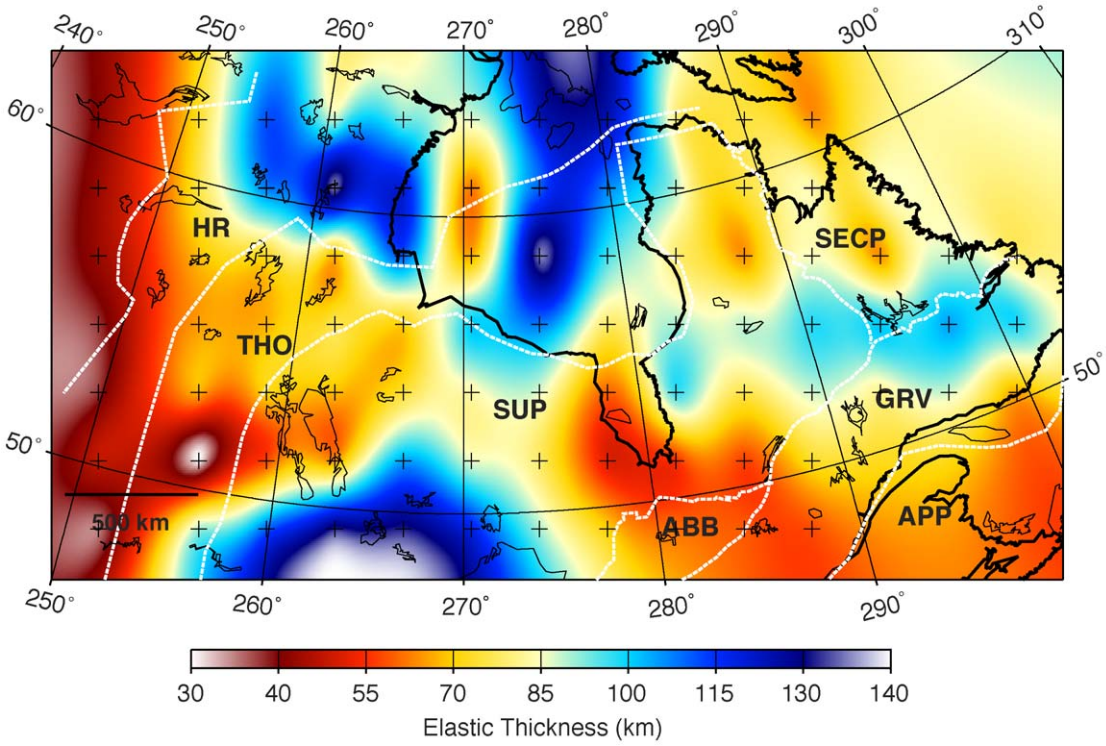

Fig. 7. T_e map of the Canadian Shield obtained with the MEM.

ince and in the Appalachian Belt to check the effect of erosion on T_e estimates. In general, f increases with decreasing wavelength and becomes meaningless for wavelengths on the order or less than the crustal thickness. For instance, in the Appalachians, f increases exponentially from 0.6 at wavelengths >600 km to ≈100 for wavelengths <60 km, in agreement with the study of Wang and Mareschal [15]. For wavelengths greater than 100 km, f is three to eight times greater in the Superior Province than in the Appalachians. This situation is due to the dominant gravity field being not expressed in the topography of the Superior Province where subsurface loads are supported by the strength of the plate and have no surface expression. In zones of active deformation, there is a rapid feedback between the tectonic uplift and denudation rates, thus only slightly increasing wavelengths of large-scale topography [34]. In cratons, this feedback is broken and the resulting topography would be over-compensated due to delayed stress relaxation, as suggested by $f(k)$ being larger in the Archean Superior Province, than in the Paleozoic Appalachians. The presence of buried loads with no surface expression (due to erosion) requires high lithospheric strength in cratonic regions [35].

4.3. Discussion

The effective elastic thickness of the continental lithosphere is determined by a combination of many factors [2]. The thermal regime of the lithosphere is only one among many controlling factors. In western Canada, the transition between the Cordillera and the Shield is marked by an increase in elastic thickness and a sharp decrease in heat flow [16]. The higher heat flow beneath the Williston and Alberta basins [36] correlates well with lower elastic thickness. The mean heat flow does not vary between provinces in the Canadian Shield but it can vary between belts with distinctive composition [37]. There is no geographic trend with heat flow being as low on the edge of the continent as in its center [38]. This absence of long wavelength trend in the thermal

regime is also reflected in our study of the variations of elastic thickness and contrasts with the conclusions by Bechtel et al. [5]. On a shorter scale, variations in elastic thickness are not clearly related to the surface heat flow. For instance, the average heat flow is lower in the Abitibi subprovince than in the rest of Superior province (37 vs. 45 mW m^{-2}) while the elastic thickness is lower in a region south and east of James Bay that includes the Abitibi. This region also includes the Kapuskasing structural zone, where crustal shortening took place along a major thrust fault. Burov et al. [35] have shown that the deep crustal faults in the Kapuskasing area reduce locally the effective elastic thickness. Furthermore, there are variations within the Abitibi, with the western Abitibi being characterized by higher heat flow and weaker lithosphere than the eastern part of the subprovince [39]. Mareschal and Jaupart [40] have shown that the amplitude of temperature variations in the mantle lithosphere could be $\pm$100 K at the base of the crust displacing mantle isotherms by $\pm$20–30 km.

Temperature in the mantle can be estimated from shear wave velocity data following the method used by Goes et al. [41]. For the Canadian Shield, Shapiro et al. [42] have inverted surface wave data together with constraints from heat flow and heat production data to determine mantle temperatures beneath the Shield. Their map does not extend further north than 60°, but some trends can be derived from a comparison with elastic thickness. For the Shield, the regions around Hudson Bay where elastic thickness is >80 km all coincide with regions where temperatures at 80-km depth have been estimated to be less than 400 °C. The correlation between elastic thickness and seismically derived mantle temperatures is not well marked for the Appalachians where temperatures at 80 km are >600 °C and where we believe that elastic thickness is high ($\approx$80 km).

The high values obtained around Hudson Bay are consistent with models that need $T_e \approx 150$ km to fit the subsidence of the Hudson Bay basin [43]. The lowest values are found in the Williston Basin (Interior Platform) where the sediment cover is thickest and has amplified the subsidence of the basin. Again, lower T_e in the Williston than in Hudson Bay is consistent with models of subsidence.

The high elastic thickness values throughout the Shield are also consistent with models of post-glacial rebound that require the elastic thickness for eastern North America to be higher than 100 km [44].

5. Conclusion

We have used three different spectral estimators (the standard windowed Fourier transform, multitaper, and maximum Entropy methods) to calculate the coherence between the Bouguer gravity field and the topography in order to estimate the variations in the elastic thickness in the Canadian Shield. Tests with synthetic data show that MEM has a higher spatial resolution and is more suited for mapping the variations in T_e, while MTM and standard Fourier transform are strongly biased to lower values and offer lower spatial resolution than MEM, depending on the window size.

The results show that T_e is lowest (30–50 km) in the Interior Platform where the Phanerozoic sediment cover is thickest, while T_e is highest beneath the Hudson Bay Basin where the sediment cover is thin. Throughout the Shield, T_e values are high (>40 km) with the highest values for the Archean Hearne–Rae provinces.

Although there is no one-to-one correspondence between T_e and surface heat flow variations, mantle temperatures estimated at 80 km are <400 °C in regions where the T_e values are high.

Acknowledgments

We are grateful to Tony Lowry for providing the MEM programs used in this study. This paper was much improved by thorough and constructive reviews by E. Burov and by a reviewer who wished to remain anonymous. We thank both of them. This work was supported by NSERC (Canada) through a postgraduate fellowship to PA and a discovery grant to J-CM.

References

[1] A.B. Watts, Isostasy and Flexure of the Lithosphere, Cambridge Univ. Press, Cambridge, UK, 2001.

[2] E.B. Burov, M. Diament, The effective elastic thickness of continental lithosphere: what does it really mean? J. Geophys. Res. 100 (1995) 3905–3927.
[3] A.B. Watts, An analysis of isostasy in the world's oceans. 1: Hawaiian-Emperor Seamount Chain, J. Geophys. Res. 83 (1978) 5989–6004.
[4] A. Lowry, R.B. Smith, Flexural rigidity of the Basin and Range–Colorado Plateau–Rocky Mountain transition from coherence analysis of gravity and topography, J. Geophys. Res. 99 (1994) 20123–20140.
[5] T.D. Bechtel, D.W. Forsyth, V.L. Sharpton, R.A.F. Grieve, Variations in effective elastic thickness of the North-American lithosphere, Nature 343 (1990) 636–638.
[6] M.K. McNutt, R.L. Parker, Isostasy in Australia and the evolution of the compensation mechanism, Science 199 (1978) 773–775.
[7] C. Beaumont, Foreland basins, Geophys. J. R. Astron. Soc. 65 (1981) 291–329.
[8] G.D. Karner, A.B. Watts, Gravity anomalies and the flexure of the lithosphere at mountain ranges, J. Geophys. Res. 88 (1983) 10449–10477.
[9] B.T.R. Lewis, L.M. Dorman, Experimental isostasy. 2: an isostatic model for the United States derived from gravity and topographic data, J. Geophys. Res. 75 (1970) 3367–3386.
[10] R.J. Banks, R.L. Parker, S.P. Huestis, Isostatic compensation on a continental scale: local versus regional mechanisms, Geophys. J. R. Astron. Soc. 51 (1977) 431–452.
[11] D.W. Forsyth, Subsurface loading and estimates of the flexural rigidity of continental lithosphere, J. Geophys. Res. 90 (1985) 12623–12632.
[12] D. McKenzie, D. Fairhead, Estimates of the effective elastic thickness of the continental lithosphere from Bouguer and free air gravity anomalies, J. Geophys. Res. 102 (1997) 27523–27552.
[13] M. Perez-Gussinye, A.R. Lowry, A.B. Watts, I. Velicogna, On the recovery of effective elastic thickness using spectral methods: examples from synthetic data and from the Fenno-scandian Shield, J. Geophys. Res. (2004) (in press).
[14] M. Pilkington, Mapping elastic thickness variations in Canada, Tectonophysics 190 (1991) 283–297.
[15] Y. Wang, J.-C. Mareschal, Elastic thickness of the lithosphere in the Central Canadian Shield, Geophys. Res. Lett. 26 (1999) 3033–3036.
[16] P. Flück, R.D. Hyndman, C. Lowe, Effective elastic thickness T_e of the lithosphere in western Canada, J. Geophys. Res. 108 (2003) 2430.
[17] F.J. Simons, R. van der Hilst, Age-dependent seismic thickness and mechanical strength of the Australian lithosphere, Geophys. Res. Lett. 29 (2002) 24.
[18] M.T. Zuber, T.D. Bechtel, D.W. Forsyth, Effective elastic thickness of the lithosphere and mechanisms of isostatic compensation in Australia, J. Geophys. Res. 94 (1989) 9353–9367.
[19] F.J. Simons, R. van der Hilst, Seismic and mechanical anisotropy and the past and present deformation of the Australian lithosphere, Earth Planet. Sci. Lett. 211 (2003) 271–286.
[20] F.J. Simons, M.T. Zuber, J. Korenaga, Isostatic response of the Australian lithosphere: estimation of effective elastic thickness and anisotropy using multitaper spectral analysis, J. Geophys. Res. 105 (2000) 19163–19184.
[21] P.F. Hoffman, Precambrian geology and tectonic history of North America, in: A.W. Bally, E.R. Palmer (Eds.), The Geology of North America: An Overview, Geol. Soc. of Am., Boulder, CO, 1989, pp. 447–512.
[22] J.F. Lewry, Z. Hajnal, A. Green, S.B. Lucas, D.J. White, M.R. Stauffer, K.E. Ashton, W. Weber, R. Clowes, Structure of a Paleoproterozoic continent–continent collision zone: a Lithoprobe seismic reflection profile across the Trans-Hudson Orogen Canada, Tectonophysics 23 (1994) 143–160.
[23] R.J. Wardle, D.T. James, D.J. Scott, J. Hall, The southeastern Churchill Province: synthesis of a PaleoProterozoic transpressional orogen, Can. J. Earth Sci. 39 (2002) 639–663.
[24] C.J. Swain, J.F. Kirby, The effect of noise on estimates of the elastic thickness of the continental lithosphere by the coherence method, Geophys. Res. Lett. 30 (2003) 1574.
[25] D. McKenzie, Estimating T_e in the presence of internal loads, J. Geophys. Res. 108 (2003) 2438.
[26] G. Ojeda, D. Whitman, Effect of windowing on lithosphere elastic thickness estimates obtained via the coherence method: results from northern South 25 America, J. Geophys. Res. 107 (2002) 2275.
[27] D.B. Percival, A.T. Walden, Spectral Analysis for Physical Applications, Cambridge Univ. Press, Cambridge, UK, 1993.
[28] J.P. Burg, A new analysis technique for time series data, in: D.G. Chiders (Ed.), Modern Spectral Analysis, IEEE Press, New York, 1978.
[29] A. Macario, A. Malinverno, W.F. Haxby, On the robustness of elastic thickness estimates obtained using the coherence method, J. Geophys. Res. 100 (1995) 15163–15172.
[30] W.H.F. Smith, D.T. Sandwell, Marine gravity field from declassified Geosat and ERS-1 altimetry EOS, Trans. - Am. Geophys. Union 76 (1995) 156.
[31] W.H.F. Smith, D.T. Sandwell, Global seafloor topography from satellite altimetry and ship depth soundings, Science 277 (1997) 1956–1962.
[32] H.C.K. Perry, D.W.S. Eaton, A.M. Forte, LITH5.0: a revised crustal model for Canada based on Lithoprobe results, Geophys. J. Int. 150 (2003) 285–294.
[33] G.D. Armstrong, A.B. Watts, Spatial variations in T_e in the southern Appalachians, eastern United States, J. Geophys. Res. 106 (2001) 22009–22026.
[34] J.P. Avouac, E.B. Burov, Erosion as a driving mechanism of intracontinental mountain growth, J. Geophys. Res. 101 (1996) 17747–17769.
[35] E. Burov, C. Jaupart, J.C. Mareschal, Large-scale heterogeneities and lithospheric strength in cratons, Earth Planet. Sci. Lett. 164 (1998) 205–219.
[36] F. Rolandone, C. Jaupart, J.C. Mareschal, C. Gariépy, G. Bienfait, C. Carbonne, R. Lapointe, Surface heat flow, crustal temperatures and mantle heat 26 flow in the Proterozoic Trans-Hudson Orogen Canadian Shield, J. Geophys. Res. 107 (2002) 2341.

[37] C. Jaupart, J.C. Mareschal, The thermal structure and thickness of continental roots, Lithos 48 (1999) 93–114.
[38] J.C. Mareschal, A. Poirier, F. Rolandone, G. Bienfait, C. Gariépy, R. Lapointe, C. Jaupart, Low mantle heat flow at the edge of the North American continent Voisey Bay, Labrador, Geophys. Res. Lett. 26 (2000) 823–826.
[39] J.C. Mareschal, C. Jaupart, C. Gariépy, L.Z. Cheng, L. Guillou-Frottier, G. Bienfait, R. Lapointe, Heat flow and deep thermal structure near the edge of the Canadian Shield, Can. J. Earth Sci. 37 (2000) 399–414.
[40] J.C. Mareschal, C. Jaupart, Variations of surface heat flow and lithospheric thermal structure beneath the North American craton, Earth Planet. Sci. Lett. 223 (2004) 650–677.
[41] S. Goes, R. Govers, P. Vacher, Shallow mantle temperatures under Europe from P and S wave tomography, J. Geophys. Res. 105 (2000) 11153–11169.
[42] N.M. Shapiro, M.H. Ritzwoller, J.C. Mareschal, C. Jaupart, Lithospheric structure of the Canadian Shield inferred from inversion of surface-wave dispersion constrained by surface heat flow, in: R.Wood, A. Curtis (Eds.), Geological Prior Information, Geol. Soc. London Spec. Publ. (in press).
[43] E. Kaminski, C. Jaupart, Lithosphere structure beneath the Phanerozoic intracratonic basins of North America, Earth Planet. Sci. Lett. 178 (2000) 139–149.
[44] W.R. Peltier, The thickness of the continental lithosphere, J. Geophys. Res. 89 (1984) 11303–11306.